PCCP

PAPER

Cite this: *Phys. Chem. Chem. Phys.*, 2017, **19**, 9566

Spontaneous NaCl-doped ice at seawater conditions: focus on the mechanisms of ion inclusion†

M. M. Conde, M. Rovere and P. Gallo *

Received 30th January 2017,
Accepted 2nd March 2017

DOI: 10.1039/c7cp00665a

rsc.li/pccp

Molecular dynamics simulations on the microsecond time scale have been performed on an aqueous solution of TIP4P/2005 water and NaCl by using the direct coexistence technique to study the ice growth and the ice/liquid interface water. At ambient pressure, for temperatures above the eutectic point of the salt and at seawater concentrations the brine rejection phenomenon and the spontaneous growth of an ice slab doped by the salt are obtained, as found in natural terrestrial and planetary environments. Experiments indicate that Cl^- goes *via* substitution to ice sites. In line with this evidence we find a new result: the Cl^- ion included in the lattice always substitutes not one but two water molecules, leaving the surrounding ice structure not distorted. The Na^+ ion shows a lower probability of being included in the ice and it occupies an interstitial site, causing a local distortion of the lattice. No signs of significant ion diffusion are observed in the lattice.

1 Introduction

Ice-doping processes are of great interest in fields such as atmospheric chemistry, astrophysics and geophysics. In recent years, various studies revealed the existence of subsurface salty oceans and the presence of high-pressure ice polymorphs in the interior of some planetary bodies such as Jupiter's satellites or exoplanets such as Proxima b.[1–5] These ices, stable over several gigapascals and hundreds of Kelvin, can contain a significant amount of small ions in their structure. The presence of doped ice suggests a plausible explanation for the behaviour and different physical properties observed in the interior of these icy bodies.

Likewise, ice formation from seawater is of great importance and it contributes to oceanic circulation so nowadays it is connected to climate change.[6–8] As seawater contains a noticeable amount of dissolved salts (mainly, Na^+ and Cl^- ions), it is very important due to the geophysical implications to study sodium chloride doping at seawater conditions.

Sodium chloride in water is the most common aqueous solution present in nature. The maximum amount of salt dissolved in water at equilibrium is given by solubility. The value of the solubility depends on the salt, the solvent, and the thermodynamic conditions (*i.e.* temperature and pressure). When it is added to ice, the salt first dissolves in the liquid water layer that is always present on the surface,[9,10] thereby lowering its freezing point below the ice coexistence temperature. Moreover, when water freezes from sea water aqueous salty solutions, the salt ions are rejected from the solid phase and saturate the liquid phase giving rise to the appearance of the phenomenon known as brine rejection. Pockets of brine form inside the polycrystalline blocks of ice. At seawater conditions the salinity is around 3.5% and below the melting point the rejected brine phase is liquid until the temperatures drop to around −21.1 °C, corresponding to the eutectic temperature of the salt.[11] At temperatures below the eutectic point the salt begins to precipitate.

In addition to the brine phase, during the ice growth a small amount of ions can be accommodated in the solid lattice causing ice doping.[12–16] The ice-doping process raises fundamental questions concerning the mechanisms by which ions are incorporated into the ice structure, and what their positions and effects are once they get there. While the properties of pure ice have been extensively studied, this has not been so for doped ice. Experiments evidenced that the presence of Na^+ and Cl^- ion dopants in the lattice modifies the properties of ice, as the incorporation of ions causes the appearance of extrinsic defects in the lattice that increase the static conductivity of the system and affect the dielectric properties of doped ice.[2–4,14,17,18] A small amount of doping impurities is sufficient to induce considerable changes in these properties.[19] Ionic defects and Bjerrum defects are in particular responsible for ice conduction. Bjerrum defects can form in pure or doped ice due to imperfect bonding between water molecules.

Dipartimento di Matematica e Fisica, Università Roma Tre, Via della Vasca Navale 84, 00146 Roma, Italy. E-mail: gallop@fis.uniroma3.it

† Electronic supplementary information (ESI) available. See DOI: 10.1039/c7cp00665a

An oxygen–oxygen bond with an extra hydrogen is called a Bjerrum D defect, an oxygen–oxygen bond with no hydrogen is called a Bjerrum L defect. These excess/missing protons favor proton motion along the lattice and therefore conduction. Ionic defects in pure or doped ice are due to weak ionization of H_2O in H_3O^+ and OH^-. NaCl belongs to the category of conductivity enhancing impurities (NaCl, HCl, HF, KF, NH_4F and others). Also, conductivity depressing impurities like NH_4OH, NH_4Cl, $NaHCO_3$ exist.

The detailed mechanisms for the doping processes in ice have not yet been fully explored. It is in fact still not clear where exactly the impurities are located in the lattice, and the location is important because it affects the concentration of defects that cause conduction.

In recent times, computer simulation has become a useful tool to draw qualitative and quantitative conclusions when applied to real systems. Molecular dynamics (MD) simulations provide a means of studying the microscopic details of these processes occurring at the molecular level, which are often difficult to study experimentally.

The goal of this work is to study the mechanism of the doping of ice at the molecular level in the presence of an aqueous solution of NaCl at seawater conditions. To perform this study we employ the direct coexistence technique where we put an ice slab in contact with an NaCl aqueous solution at seawater concentration. Since the pioneering works of Ladd and Woodcock[20,21] this technique has been implemented successfully in a large number of systems.[22–25] In particular Vrbka and Jungwirth[26,27] employed this technique to study the brine rejection phenomenon. They investigated freezing, observing brine rejection in solutions of water and NaCl with varying salt concentrations and they observed a correlation between the value of the salt concentration of the solution as ice formation progresses and the velocity of the formation of the freezing front. The more the solution is concentrated the slower the ice front progresses. They could not study ion inclusions because the system was too small.

The present paper is organized as follows: in the next section force fields are described, and the third section explains the construction of the starting configuration and the details of the time evolution of the simulations. In the fourth section we describe in detail the dynamics and evolution of the ice-doping process. The fifth section analyzes in detail the mechanism of inclusion of the two ionic species. Finally, the main conclusions are discussed.

Table 1 Force field parameters of the TIP4P/2005 water model[28] and NaCl model[31]

Site	C_6 (kJ mol^{-1} nm^6)	C_{12} (kJ mol^{-1} nm^{12})	q (e)
O	0.30798×10^{-2}	0.30601×10^{-5}	—
H	—	—	+0.5564
M	—	—	−1.1128
Na^+	—	0.83200×10^{-7}	+1
Cl^-	—	0.52000×10^{-4}	−1
Na^+–O	0.08000×10^{-2}	2.09430×10^{-7}	—
Cl^-–O	0.15000×10^{-2}	1.64480×10^{-5}	—

2 Force fields

For our system of ice/NaCl(aq), the water molecules were modelled using the well-known rigid nonpolarizable TIP4P/2005 potential.[28] This potential has been successfully used to describe water behaviour all over the phase diagram, see for example ref. 29 and 30 and references therein. In TIP4P/2005 a Lennard-Jones interaction site is located on the oxygen atom, positive charges are located on the positions of the hydrogen atoms, and the negative charge is located at a distance d_{OH} = 0.1546 Å from the oxygen along the H–O–H bisector. It is well known that the melting point of this potential at ambient pressure is 250 K.[25,28] In our simulations we used a very recent new set of parameters for the ion–water and ion–ion interactions proposed by Vega and co-workers,[31] fitted to reproduce the solubility of NaCl in water. The value of the solubility obtained for this new set of parameters at normal conditions for p and T is 5.8 m (moles of salt per kilogram of water, denoted as molality (m)) in good agreement with the experimental value. The experimental solubility for NaCl in water at 298.15 K and 1 bar is 6.14 m.[32] This agreement is particularly important for the combined use with TIP4P/2005 as the solvent–ion interaction parameters are compensating for the slight difference in mobility between TIP4P/2005 and experimental water.

The potential parameters for both models as well as the cross interactions between the ions and the oxygen in water are given in Table 1. The geometry of the water molecules was enforced using constraints. The Lennard-Jones part of the potential was truncated at 8.5 Å. Ewald sums were used to deal with electrostatics.[33] The real part of the Coulombic potential was truncated at 8.5 Å. The width of the mesh was 1 Å and we used a fourth order polynomial.

3 Initial configuration preparation and systems evolution

In order to generate the initial configuration for the system formed by ice and liquid water in the presence of NaCl we began building an equilibrated slab of ice I_h of 2000 water molecules. Periodic boundary conditions were employed in the three directions of space. We used the algorithm proposed by Buch *et al.*[34] to obtain a configuration with proton disorder and almost zero dipole moment satisfying the Bernal–Fowler rules.[35] The initial solid configuration was equilibrated over about 50 ns at ambient pressure allowing the three different sides of the simulation box to fluctuate independently to avoid stress in the solid lattice. The dimensions of the equilibrated ice slab were 45 Å × 38.97 Å × 36.74 Å. Once the ice was equilibrated we built the box for the liquid phase corresponding to the NaCl solution at seawater concentration. Starting from the previous ice configuration and replicating it four times in the direction x we performed an *NVT* simulation about over 10 ns at 400 K to melt it completely obtaining a configuration of 8000 liquid water molecules. Salt was introduced into the liquid phase until the desired seawater molar concentration was reached (0.599 M, 1 bar). 87 NaCl ion pairs were necessary to obtain a molar concentration of 0.599 M.

We performed a Np_xT simulation over about 50 ns to equilibrate the NaCl(aq) phase. The final size of the simulation box for the NaCl solution was 168.23 Å × 38.97 Å × 36.74 Å. Next, we put the solid in contact with the liquid phase. The plane of ice I_h exposed at the interface was the secondary prismatic plane $(1\bar{2}10)$ since it has been shown that this plane exhibits the fastest dynamics.[36,37] Thus, the initial configuration was formed by a slab of ice I_h which acts as seed crystal in contact with a water liquid phase containing Na^+ and Cl^- ions in solution at 0.599 M (seawater concentration). The resulting box contained 2000 water molecules in the ice phase, 8000 water molecules in the liquid phase and 87 NaCl ion pairs.

Finally, we equilibrated the system for a short time (20 ps) in order to have an equilibrated interface. The size of the initial configuration was 216.88 Å × 38.97 Å × 36.74 Å.

In our study we used a very large size for the sample, more than 10 000 molecules, to reduce significantly the effects due to the stochastic nature of the direct coexistence simulations and the finite size effects.[38] Fig. 1 shows a snapshot of the initial configuration used in this study for the system of ice/NaCl(aq). All of the direct coexistence simulations for our study were performed in the Np_xT ensemble using the molecular dynamics package GROMACS (version 4.5.5).[39] The choice of the Np_xT ensemble where the pressure is applied only in the direction perpendicular to the interface (in our system the x-axis) is due to the fact that this is the ensemble that is strictly correct for the direct coexistence simulations.[38,40] The temperature was fixed using the Nosé–Hoover thermostat[41,42] with a relaxation time of 2 ps. To keep the pressure constant, a Parrinello–Rahman barostat[43] was used. The relaxation time of the barostat was 2 ps. The time-step used in the simulations was 2 fs. The data presented in this paper resulted from a calculation that would last 70 years on a single processor. We studied four different temperatures below the melting point of water and above the eutectic point. The temperatures chosen were $\Delta T = -5$ K, -10 K, -15 K and -20 K where ΔT is the difference between the temperature of the system and the melting temperature. We used the same initial configuration for all temperatures. The length of each simulation was 2 μs.

4 Spontaneous doped ice growth

We now analyze the results for doped ice growth obtained using the direct coexistence technique for the four temperatures studied.

Fig. 2 shows the time evolution of the potential energy as a function of time for the four simulations. For all of the temperatures analyzed we observe a decrease in the potential energy indicating the growth of an ice slab and the phase transition from liquid water to ice phase. The melting point of water in the presence of NaCl differs from that of pure water. Experimentally, the melting point at seawater concentration drops by around 2 K. At $\Delta T = -10$ K, -15 K and -20 K a continuous decrease of the energy is observed up to 1 μs and then it remains constant until the end of the run. The final plateau in the energy indicates that the system has reached the equilibrium state. At $\Delta T = -5$ K the energy continues to fall slowly and a longer period of simulation would be necessary to reach the final state of equilibrium. In any case, our goal in this study is not to reach the final state but to have a sample of doped ice big enough to analyze the mechanism

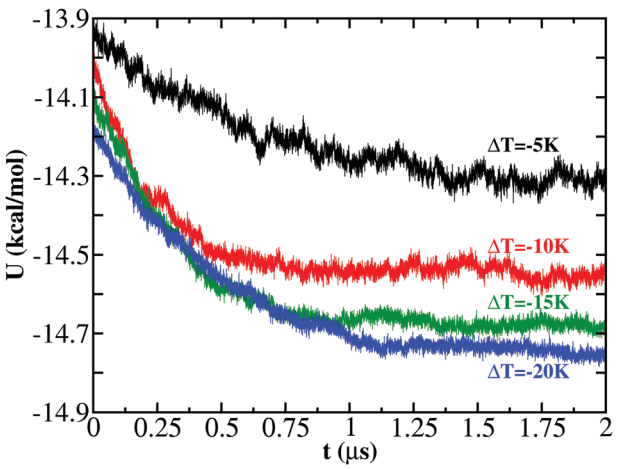

Fig. 2 Potential energy as a function of time obtained at several temperatures for the ice/NaCl(aq) system. $\Delta T = T_m - T$ where T_m is the melting temperature for the TIP4P/2005 water model and T is the temperature of the system.

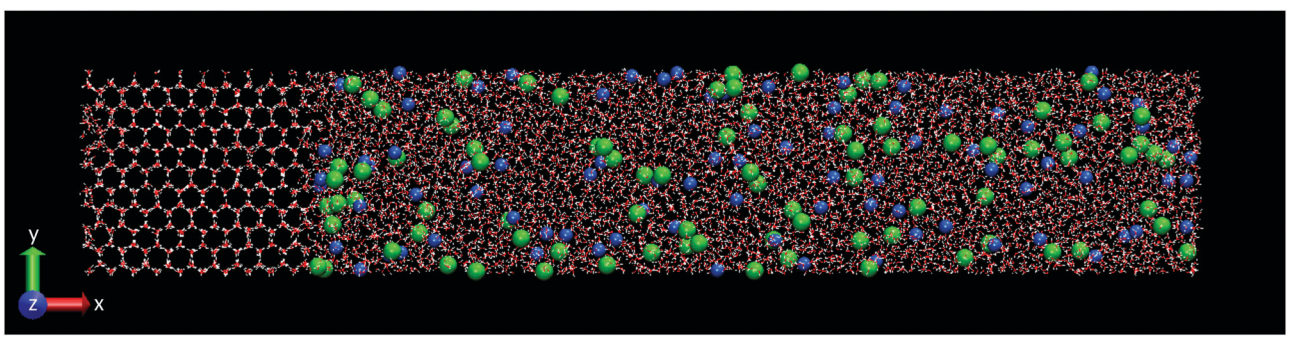

Fig. 1 XY projection of a snapshot of the initial configuration formed by a slab of ice I_h and a NaCl aqueous solution at seawater concentration. The plane of ice I_h exposed at the interface is the secondary prismatic plane. The plane that can be seen is the basal plane. Water molecules are plotted in red and white colors, Cl^- ions are plotted in green and Na^+ ions are plotted in blue. The size of the ions is enlarged with respect to the water molecules for a clearer visualization.

of the spontaneous inclusion of the ions in the ice lattice. In all four cases we have achieved our goal. The rate of the decrease of the potential energy can already give us an idea of the velocity of the growth of the ice front in the sample. We note that for all of the four temperatures studied initially there is a steep decrease indicating that ice is growing very fast and the potential energy decrease gradually slows down.

In Fig. 3(a)–(d) we show the snapshots of the final configurations and in the ESI† we show the movie of one of the four simulations at −20 K. At temperatures below the melting point in a pure water system the water freezes forming a unique phase of ice when reaching the equilibrium state. However the presence of salt and its low solubility in the ice[18] causes the appearance of the natural phenomenon of brine rejection where the salt ions are rejected from the ice lattice and forced out into the liquid phase of the system which becomes brine.

In all of the four final configurations we can clearly see the presence of the rejected brine. The volume occupied by the brine phase of a glassy nature[26] is different for each temperature studied and depends on the difference between the simulation temperature and the melting temperature.[16,44] The volume is larger for temperatures closer to the melting point. At temperatures far below the melting point it was found that the freezing of the system was completed, as reported by Vrbka and Jungwirth for smaller systems and lower concentrations of salt.[26,27] A visual observation of the final configurations shows the spontaneous growth of a slab of ice doped by salt ions.

The ions are obviously located only in the new slab of ice formed and not in the initial ice used as seed crystal. No special patterns are found in the distribution of the ions along the lattice. Ions appear to be randomly placed in the doped ice.

From the movie in the ESI† we can see the ice growth, the ion inclusion and the remaining rejected brine at the end of the run. Similarly to what was found by Vrbka and Jungwirth,[26,27] the velocity of the formation of the ice front in contact with the aqueous solution decreases with the increasing salt content in the solution.

Another important issue is the preferential incorporation of ions into the ice structure. At temperatures close to the melting point ($\Delta T = -5$ K and -10 K) the slab of grown ice is doped only by Cl^- ions. However, when the change in temperature with respect to the melting point is -15 K and -20 K some Na^+ ions are also incorporated into the lattice, although Cl^- ions always enter the ice lattice in much higher proportions than Na^+ ions. This preferential incorporation is in agreement with that reported in experimental studies.[45–47] In fact, this preference explains the increase in static conductivity when these types of dopant ions are present in the ice.[47,48] In Table 2 the ion concentrations in the doped ice and the brine phase are given.

To estimate the number of ions present in each phase we selected, for a number of equilibrated configurations, for all of the temperatures studied, the slab of ice grown (discarding the initial pure ice slab of 2000 molecules) and the brine phase. Equilibrated configurations are selected in the time frame where the potential energy shows a constant behaviour (see Fig. 2).

The errors were calculated as maxima errors for the number of water molecules and ions belonging to one of the two phases, and with the propagation of error for the calculation of the concentration.

As can be seen in Table 2, the number of included ions decreases at temperatures close to the melting point. The cation is preferentially excluded from the solid lattice and its concentration in the ice is lower than the anion. Consequently, the doped ice slab acquires an excess of negative charge and the brine phase is positively charged due to the larger number of Na^+ in that phase. Experimentally, the maximum concentration of Cl^- ions present in the ice lattice has been determined[47] to lie in the range 10^{-3}–10^{-5} M for initial NaCl solutions of the order 10^{-2}–10^{-4} M. Our initial NaCl solution is more concentrated, but through extrapolating the numbers our results appear to provide a good prediction of the concentration of Cl^- dopants in ice.

5 Mechanism of inclusion for Na^+ and Cl^- in the ice I_h

In order to identify the positions of the ions in the doped ice lattice we selected, from the final configurations obtained, samples of ice doped by Cl^- and Na^+. For a better visual understanding of the ion positions in the lattice we show these doped ice samples and a sample of equilibrated pure ice in Fig. 4–7. Frontal views of snapshots in the basal, secondary and primary prismatic projections are shown for the pure ice, two configurations of Cl-doped ice and one configuration of Na-doped ice.

The pure ice I_h sample is shown in Fig. 4 for the three chosen views. It is formed by a total of 26 water molecules distributed in two layers of three hexagonal rings each. The hexagonal channels arranged in planes and the proton disorder of the ice structure can be clearly seen. The lattice is perfect, with no defects and only thermal motion is slightly displacing the molecules from their lattice equilibrium positions.

In all of our simulations when a Cl^- ion is doping the ice the number of water molecules in the portion that we selected is reduced from 26 to 24. This can be seen in Fig. 5 and 6. In both sets of figures we observe that apart from the two missing water molecules the structure of the lattice is undistorted. These observations indicate that the Cl^- ion substitutes two water molecules in such a way that, although it does not sit on a lattice site, it energetically acts as if the two water molecules that it is replacing were still there. As the ionic radius of the Cl^- (167 pm) is approximately twice the radius of the oxygen (73 pm), and the oxygen is also engaged in bonding two hydrogens, it seems understandable that one Cl^- ion is able to substitute two water molecules while keeping the ice structure stable. Due to the presence of the Cl^- we also observe that the protons of the nearby water molecules are oriented toward the ion. By analyzing all of the positions of the Cl^- ions included in our four simulations we found that the Cl^- occupies only two kind of positions in the ice lattice. By far the more frequent one is

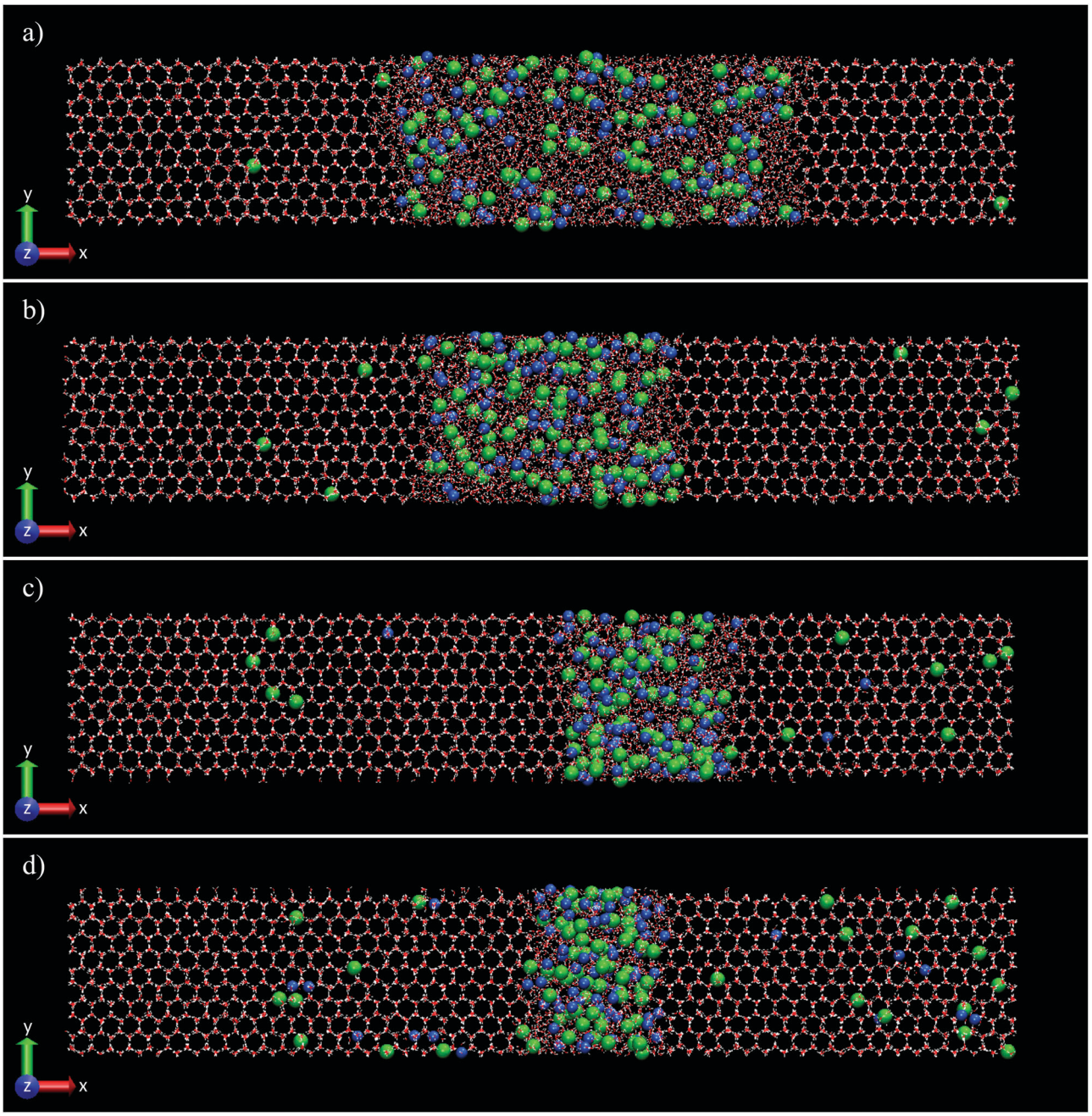

Fig. 3 Final snapshots for the ice/NaCl(aq) system after 2 μs at different temperatures. (a) $\Delta T = -5$ K, (b) $\Delta T = -10$ K, (c) $\Delta T = -15$ K and (d) $\Delta T = -20$ K. Water molecules are plotted in red and white colors, Cl^- ions are plotted in green and Na^+ ions are plotted in blue. The sizes of the ions are enlarged with respect to the water molecules for a clearer visualization.

Table 2 Ion concentrations in the doped ice and the brine phase at the temperatures studied. ΔT is the difference between the temperature of the system and the melting temperature. n_{ice}^{grown} is the number of molecules obtained in the grown ice by direct coexistence. n_{Cl^-} and n_{Na^+} are the number of chloride and sodium ions, respectively, present in the grown ice and the brine phase. Concentrations are given in mol L^{-1}

ΔT (K)	n_{ice}^{grown}	$n_{Cl^-}^{ice}$	$n_{Na^+}^{ice}$	$[Cl^-]_{ice}$	$[Na^+]_{ice}$	$n_{Cl^-}^{brine}$	$n_{Na^+}^{brine}$	$[Cl^-]_{brine}$	$[Na^+]_{brine}$
−5	3493 ± 213	2 ± 0	—	(257 740 ± 9) × 10^{-7}	—	85 ± 1	87 ± 0	(74 124 ± 4) × 10^{-5}	(75 868 ± 3) × 10^{-5}
−10	5075 ± 139	6 ± 1	—	(57 040 ± 7) × 10^{-6}	—	81 ± 1	87 ± 0	(93 015 ± 3) × 10^{-5}	(99 905 ± 3) × 10^{-5}
−15	5929 ± 206	10 ± 1	3 ± 1	(82 257 ± 7) × 10^{-6}	(24 677 ± 6) × 10^{-6}	77 ± 1	84 ± 1	(104 936 ± 5) × 10^{-5}	(115 982 ± 3) × 10^{-5}
−20	6266 ± 142	21 ± 1	13 ± 1	(172 405 ± 7) × 10^{-6}	(109 712 ± 6) × 10^{-6}	66 ± 1	74 ± 1	(99 195 ± 6) × 10^{-5}	(111 404 ± 3) × 10^{-5}

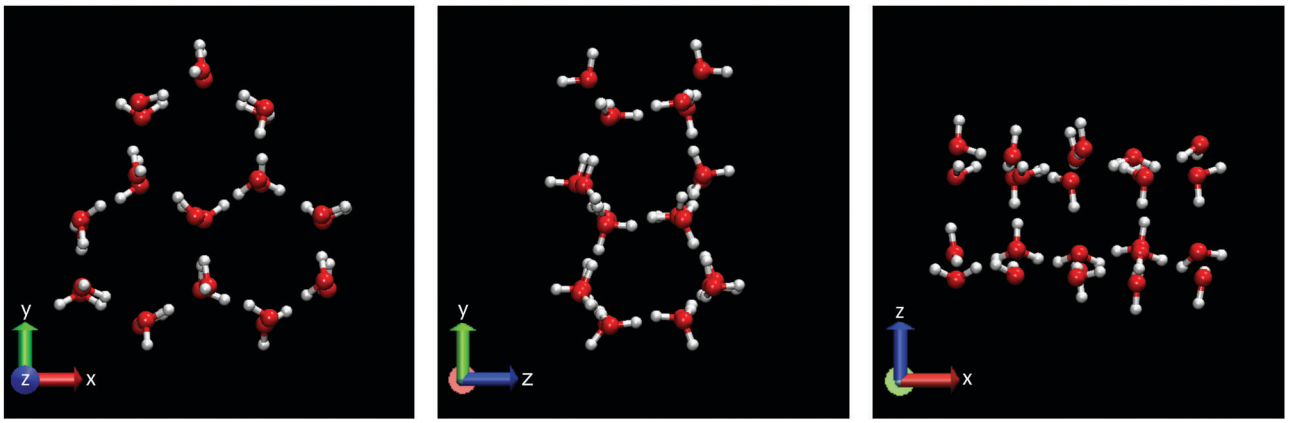

Fig. 4 Snapshot of a pure ice I_h lattice portion made of three hexagonal rings and two planes. Frontal view of the basal (left), secondary prismatic (center) and primary prismatic (right) projections. The ice sample is obtained at $\Delta T = -15$ K. Water molecules are plotted in red and white colors.

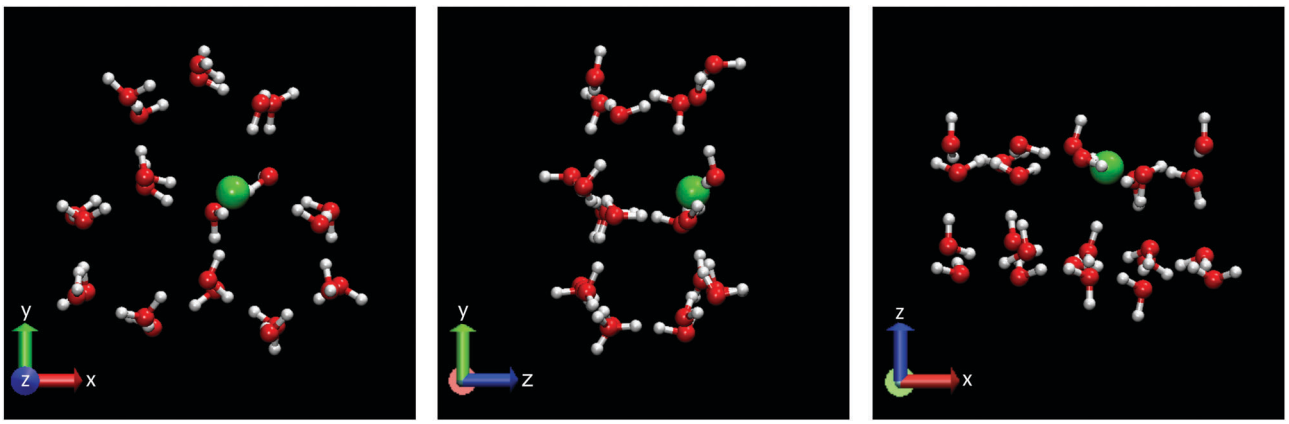

Fig. 5 Snapshot of a doped ice I_h lattice portion made of three hexagonal rings and two planes and containing a Cl^- ion laying in the plane made of hexagonal rings. Frontal view of the basal (left), secondary prismatic (center) and primary prismatic (right) projections. The doped ice sample is obtained at $\Delta T = -15$ K. Water molecules are plotted in red and white colors, the Cl^- ion is plotted in green. Particles are represented so that the relative size is correct. We considered the atoms and the ion as spheres whose radii are the atomic and ionic radii respectively.

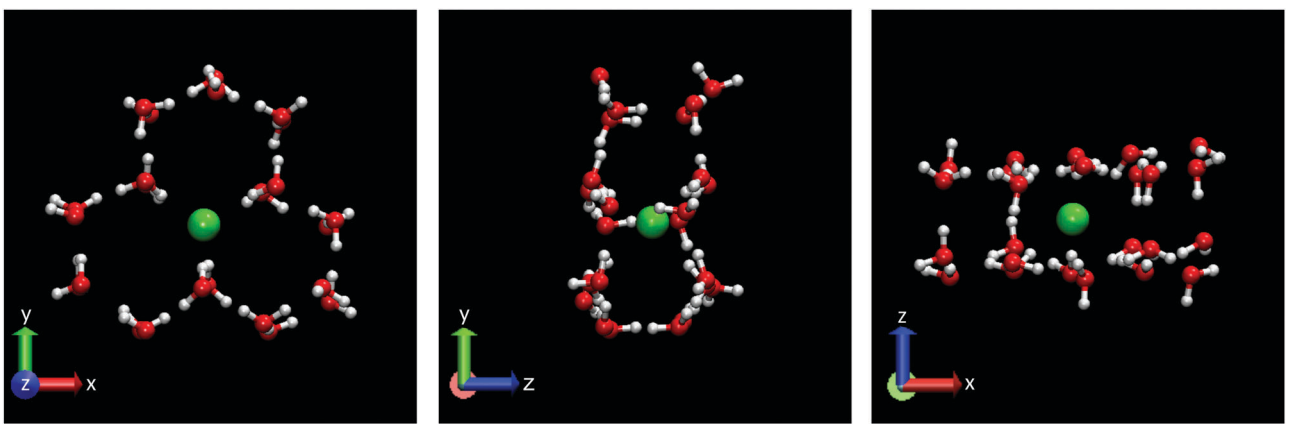

Fig. 6 Snapshot of a doped ice I_h lattice portion made of three hexagonal rings and two planes and containing a Cl^- ion laying between two adjacent planes of hexagonal rings. Frontal view of the basal (left), secondary prismatic (center) and primary prismatic (right) projections. The doped ice sample is obtained at $\Delta T = -15$ K. Water molecules are plotted in red and white colors, the Cl^- ion is plotted in green. Particles are represented so that the relative size is correct. We considered the atoms and the ion as spheres whose radii are the atomic and ionic radii respectively.

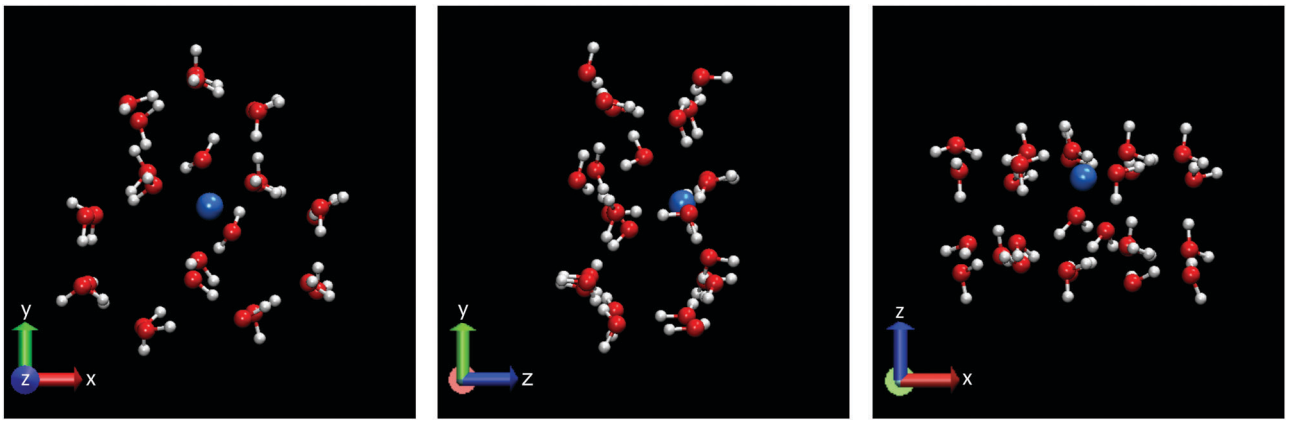

Fig. 7 Snapshot of a doped ice I_h lattice portion made of three hexagonal rings and two planes and containing a Na^+ ion. Frontal view of the basal (left), secondary prismatic (center) and primary prismatic (right) projections. The doped ice sample is obtained at $\Delta T = -15$ K. Water molecules are plotted in red and white colors, the Na^+ ion is plotted in blue. Particles are represented so that the relative size is correct. We considered the atoms and the ion as spheres whose radii are the atomic and ionic radii respectively.

when the Cl^- substitutes two nearest neighbour water molecules belonging to the same plane. Out of 39 Cl^- ions doping our four slabs of ice, 36 were in this configuration, which is shown in Fig. 5. In our lattices we found only three Cl^- ions that substituted two nearest neighbour water molecules belonging to two adjacent planes. Although much less likely, this position is nonetheless energetically allowed. This configuration is shown in Fig. 6. The three views shown in these figures allow the location of the exact position of the ions, and the comparison with the pure ice lattice of Fig. 4 allows us to identify the two missing water molecules.

Experimentally indirect evidence from conductivity and dielectric constant measurements[19,45] was found that the Cl^- is incorporated into an undistorted ice lattice creating an L-type Bjerrum defect. An L-Bjerrum defect consists of an ice site where the hydrogen bond has no protons. It is in fact known that L defects are released into the lattice, one for each missing hydrogen, when ions like Cl^- and F^- are substitutional defects in ice; for more details see for example ref. 18. These missing protons favor proton motion along the lattice and therefore conduction. As is evident from the figures, our results reveal a novel mechanism where one Cl^- ion substitutes not one but two water molecules. This is compatible with the experimental results and creates L defects. Additionally, our results give an important microscopic insight on the doped crystal structure.

As a small percentage of Na^+ ions are also included in the two lowest temperature simulations we now show that the position of the ion is always in the same kind of portion of the lattice, namely two adjacent layers of three hexagonal rings each. In Fig. 7 we show the sample when the dopant is the Na^+ ion. We observe that in all cases found in our simulations the number of water molecules is equal to 26, namely the number of water molecules contained in the sample of pure ice. We observe that in this case, the Na^+ ion occupies an interstitial site and its presence causes a quite relevant local distortion of the ice lattice. In more detail we observe that two water molecules leave their lattice equilibrium position to get closer to the off-lattice Na^+ dopant. Na^+ has an ionic radius (116 pm) closer to the radius of oxygen. Also in this case we note that the proton disorder of the lattice is maintained, however the protons close to the sodium orient themselves away from the positive ion. In contrast with the Cl^- the position of the Na^+ is in the plane of the hexagons for of all the inclusions that we found for this ion.

After analyzing the trajectories we observed that there is no significant diffusion of the ions along the solid lattice, in agreement with experimental evidence found by Gross *et al.*[14] For our timescale, which is that of microseconds, for the Cl^- ions incorporated in the lattice we only observe switches between two equilibrium positions inside the cell. Also the Na^+ ions do not diffuse on this timescale, they only move inside the hexagonal rings. These movements can also be observed in the movie in the ESI.†

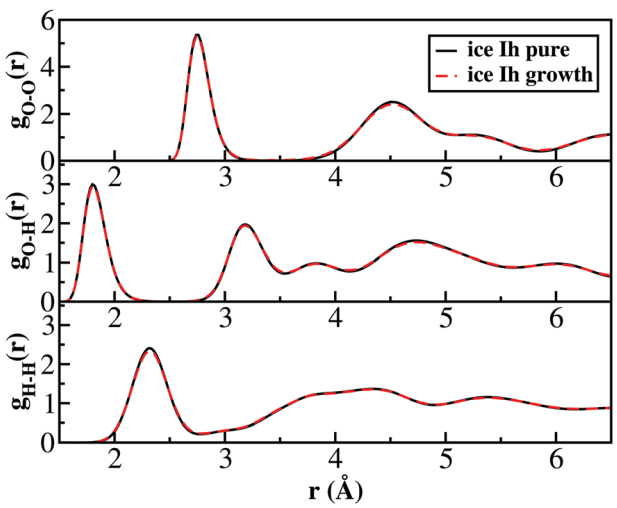

Fig. 8 Oxygen–oxygen, oxygen–hydrogen and hydrogen–hydrogen radial distribution functions for a slab of pure ice I_h (solid line) and for the doped ice grown *via* direct coexistence (dashed line). The radial distribution functions of doped ice were obtained at $\Delta T = -10$ K and at 1 bar.

In order to verify that the ice lattice is not globally distorted by these inclusions we computed the oxygen–oxygen, oxygen–hydrogen and hydrogen–hydrogen radial distribution functions for the ice I_h used as seed and for the ice grown through direct coexistence at $\Delta T = -10$ K at 1 bar. We show in Fig. 8 that the radial distribution functions of pure and doped ices are practically identical and this also provides structural evidence that the solid phase obtained through direct coexistence with the NaCl aqueous solution is ice I_h. The local distortions due to Na^+ are not statistically important because Na^+ has a very low probability of inclusion. The same radial distribution functions were obtained for the other three thermodynamic states studied (not shown).

6 Conclusions

In summary, in this paper we studied the mechanism of spontaneous NaCl-doped ice at seawater conditions. Long time simulations on a microsecond scale were performed in order to produce four slabs of doped ice. The decrease of the potential energy as a function of time and visual inspection of the simulation trajectories indicate the growth of an ice slab and the phase transition from liquid water to ice phase. A brine phase at temperatures below the melting point was found. The volume occupied by this phase is different for each temperature studied and depends on the difference between the simulated temperature and the melting temperature, being larger for temperatures closer to the melting point. The velocity of the growth of the ice front decreases as the concentration of the ions in the liquid phase increases. The Cl^- ion is preferentially incorporated in the solid lattice and only for the lowest temperatures simulated could very few Na^+ ions be incorporated. This preference explains the increase in static conductivity when these types of dopant ions are present in the ice. As for the positions that these ions occupy in the lattice, while Na^+ ions dope the ice interstitially as expected, meaning that we basically confirmed what is hypothesized in the literature, we show here to the best of our knowledge for the first time the microscopic doping mechanism for the Cl^- ion. In the literature there is only indirect evidence that it is incorporated in the ice lattice. We found here that Cl^- substitutes not one but two water molecules in the lattice without distorting it. The included Cl^- preferentially sits in the hexagonal ring plane but it can also sit between two adjacent planes. These findings have important implications for the electrical properties of doped ice. The defects that this ion causes are Bjerrum L defects, which imply the presence of conduction *via* proton transfer. When the ice is doped by the cation or the anion the proton disorder is maintained along the ice lattice. However, in the environment of the dopant the water molecules are re-oriented according to the charge of the ion. When the dopant is the Cl^- the protons of the nearby water molecules are oriented towards the ion and in the opposite direction in the case of Na^+.

It would be interesting to study whether this mechanism of substitution of two water molecules also happens for some other anions belonging to the class of conductivity enhancing impurities. In the future we plan to perform simulations on this issue.

Acknowledgements

We thank Carlos Vega and co-workers for having provided the NaCl-TIP4P/2005 interaction parameters to us prior to publication of their paper.

References

1 M. R. Frank, C. E. Runge, H. P. Scott, S. J. Maglio, J. Olson, V. B. Prakapenka and G. Shen, *Phys. Earth Planet. Inter.*, 2006, **155**, 152.
2 S. Klotz, L. E. Bove, T. Strässle, T. C. Hansen and A. M. Saitta, *Nat. Mater.*, 2009, **8**, 405.
3 L. E. Bove, R. Gaal, Z. Raza, A. A. Ludl, S. Klotz, A. M. Saitta, A. F. Goncharov and P. Gillet, *Proc. Natl. Acad. Sci. U. S. A.*, 2015, **112**, 8216.
4 E. Pettinelli, B. Cosciotti, F. D. Paolo, S. E. Lauro, E. Mattei, R. Orosei and G. Vannaroni, *Rev. Geophys.*, 2015, **53**, 593.
5 B. Brugger, O. Mousis, M. Deleuil and J. I. Lunine, *Astrophys. J., Lett.*, 2015, **831**, L16.
6 K. Aagaard and E. C. Carmack, *J. Geophys. Res.*, 1989, **94**, 14485.
7 A. Y. Shcherbina, L. D. Talley and D. L. Rudnick, *Science*, 2003, **302**, 1952.
8 K. I. Ohshima, Y. Fukamachi, G. D. Williams, S. Nihashi, F. Roquet, Y. Kitade, T. Tamura, D. Hirano, L. Herraiz-Borreguero, I. Field, M. Hindell, S. Aoki and M. Wakatsuchi, *Nat. Geosci.*, 2013, **6**, 235.
9 M. Faraday, *Proc. R. Soc. London*, 1860, **10**, 440.
10 J. W. M. Frenken and J. F. van der Veen, *Phys. Rev. Lett.*, 1985, **54**, 134.
11 R. E. Dickerson, *Molecular Thermodynamics*, W. A. Benjamin, Pasadena, 1969.
12 E. L. Workman and S. E. Reynolds, *Phys. Rev.*, 1950, **78**, 254.
13 G. W. Gross, *Ann. N. Y. Acad. Sci.*, 1965, **125**, 380.
14 G. W. Gross, *Adv. Chem.*, 1968, **73**, 27.
15 A. W. Cobb and G. W. Gross, *J. Electrochem. Soc.*, 1969, **116**, 796.
16 J. R. Addison, *J. Appl. Phys.*, 1969, **40**, 3105.
17 N. H. Fletcher, *The Chemical Physics of Ice*, Cambridge University Press, 1970.
18 V. F. Petrenko and R. W. Whitworth, *Physics of Ice*, Oxford University Press, 1999.
19 J. Moore, J. Paren and H. Oerter, *J. Geophys. Res.*, 1992, **97**, 19803.
20 A. J. C. Ladd and L. Woodcock, *Chem. Phys. Lett.*, 1977, **51**, 155.
21 A. J. C. Ladd and L. Woodcock, *Mol. Phys.*, 1978, **36**, 611.
22 O. A. Karim, P. A. Kay and A. D. J. Haymet, *J. Chem. Phys.*, 1990, **92**, 4634.

23 R. G. Fernandez, J. L. F. Abascal and C. Vega, *J. Chem. Phys.*, 2006, **124**, 144506.
24 M. M. Conde and C. Vega, *J. Chem. Phys.*, 2010, **133**, 064507.
25 M. M. Conde, M. A. Gonzalez, J. L. F. Abascal and C. Vega, *J. Chem. Phys.*, 2013, **139**, 154505.
26 L. Vrbka and P. Jungwirth, *Phys. Rev. Lett.*, 2005, **95**, 148501.
27 L. Vrbka and P. Jungwirth, *J. Mol. Liq.*, 2007, **134**, 64.
28 J. L. F. Abascal and C. Vega, *J. Chem. Phys.*, 2005, **123**, 234505.
29 C. Vega, J. L. F. Abascal, M. M. Conde and J. L. Aragones, *Faraday Discuss.*, 2009, **141**, 251.
30 P. Gallo, K. Amann-Winkel, C. A. Angell, M. A. Anisimov, F. Caupin, C. Chakravarty, E. Lascaris, T. Loerting, A. Z. Panagiotopoulos, J. Russo, J. A. Sellberg, H. E. Stanley, H. Tanaka, C. Vega, L. Xu and L. G. M. Pettersson, *Chem. Rev.*, 2016, **116**, 7463.
31 C. Vega, private communication, 2016.
32 P. Cohen, *Handbook on Water Technology for Thermal Power Systems*, ASME, New York, 1989.
33 U. Essmann, L. Perera, M. L. Berkowitz, T. Darden, H. Lee and L. G. Pedersen, *J. Chem. Phys.*, 1995, **103**, 8577.
34 V. Buch, P. Sandler and J. Sadlej, *J. Phys. Chem. B*, 1998, **102**, 8641.
35 J. D. Bernal and R. H. Fowler, *J. Chem. Phys.*, 1933, **1**, 515.
36 H. Nada and Y. Furukawa, *J. Cryst. Growth*, 2005, **283**, 242.
37 M. M. Conde, C. Vega and A. Patrykiejew, *J. Chem. Phys.*, 2008, **129**, 014702.
38 J. R. Espinosa, E. Sanz, C. Valeriani and C. Vega, *J. Chem. Phys.*, 2013, **139**, 144502.
39 D. van Der Spoel, E. Lindahl, B. Hess, G. Groenhof, A. E. Mark and H. J. C. Berendsen, *J. Comput. Chem.*, 2005, **26**, 1701.
40 D. Frenkel, *Eur. Phys. J. Plus*, 2013, **128**, 10.
41 S. Nosé, *J. Chem. Phys.*, 1984, **81**, 511.
42 W. G. Hoover, *Phys. Rev. A: At., Mol., Opt. Phys.*, 1985, **31**, 1695.
43 M. Parrinello and A. Rahman, *J. Appl. Phys.*, 1981, **52**, 7182.
44 J. Moore, A. P. Reid and J. Kipfstuhl, *J. Geophys. Res.*, 1994, **99**, 5171.
45 N. Maeno, *Can. J. Phys.*, 1973, **51**, 1045.
46 G. W. Gross, I. C. Hayslip and R. N. Hoy, *J. Glaciol.*, 1978, **21**, 143.
47 N. W. Riley, G. Noll and J. W. Glen, *J. Glaciol.*, 1978, **21**, 501.
48 R. E. Grimm, D. E. Stillman, S. F. Dec and M. A. Bullock, *J. Phys. Chem. B*, 2008, **112**, 15382.